MIT Open Access Articles

Efficient resonance assignment of proteins in MAS NMR by simultaneous intra- and inter-residue 3D correlation spectroscopy

Massachusetts Institute of Technology

Efficient Resonance Assignment of Proteins in MAS NMR by Simultaneous Intra- and Inter-residue 3D Correlation Spectroscopy

Eugenio Daviso[1,2], **Matthew T. Eddy**[2], **Loren B. Andreas**[2], **Robert G. Griffin**[2], and **Judith Herzfeld**[1,Ŧ]

[1]Department of Chemistry, Brandeis University, Waltham, Massachusetts, USA, 02454-9110

[2]Francis Bitter Magnet Laboratory and Department of Chemistry, Massachusetts Institute of Technology, Cambridge, Massachusetts, USA, 02139

Abstract

Resonance assignment is the first step in NMR structure determination. For magic angle spinning NMR, this is typically achieved with a set of heteronuclear correlation experiments (NCaCX, NCOCX, CONCa) that utilize SPECIFIC-CP ^{15}N-^{13}C transfers. However, the SPECIFIC-CP transfer efficiency is often compromised by molecular dynamics and probe performance. Here we show that one-bond ZF-TEDOR ^{15}N-^{13}C transfers provide simultaneous NCO and NCa transfers with at least as much sensitivity as SPECIFIC-CP for some non-crystalline samples. Furthermore, a 3D TEDOR-CC experiment provides heteronuclear sidechains correlations and robustness with respect to proton decoupling and radiofrequency power instabilities. We demonstrate transfer efficiencies and connectivities by application of 3D ZF-TEDOR-DARR to a model microcrystalline protein, GB1, and a less ideal system, GvpA in intact gas vesicles.

Keywords

3D MAS NMR; TEDOR; DARR; sidechain-backbone correlation

Introduction

Magic angle spinning nuclear magnetic resonance (MAS NMR) is a burgeoning approach to characterizing the structure and dynamics of such otherwise intractable systems as membrane proteins (Andreas et al. 2012; Andreas et al. 2010; Higman et al. 2009; Eddy et al. 2012a; Ader et al. 2010; Bhate et al. 2010; Higman et al. 2011; Li et al. 2008; Renault et al. 2011; Varga et al. 2007), and amyloid fibrils (Bateman et al. 2011; Bayro et al. 2012; Bayro et al. 2011; Bayro et al. 2010; Debelouchina et al. 2010a, b; Hu et al. 2011; Jaroniec et al. 2002a; Kryndushkin et al. 2011; Comellas et al. 2012; Lemkau et al. 2012; Li et al. 2011; Lv et al. 2012; Paravastu et al. 2008; Paravastu et al. 2009; Qiang et al. 2012; Sivanandam et al. 2011; Van Melckebeke et al. 2010; Wasmer et al. 2008). To date, twenty-five unique protein structures determined by MAS NMR have been deposited in the protein data bank (Bernstein et al. 1977; Warschawski 2011) and further advances in NMR methodology, high field instrumentation, and sensitivity-enhancing techniques, such as dynamic nuclear polarization, promise to increase this number dramatically in the near future.

ŦCorresponding author: Judith Herzfeld, herzfeld@brandeis.edu.

The first step in determining a protein structure by NMR is identifying and assigning individual nuclear resonances. For large biomolecules this often requires 3D heteronuclear experiments to remove degeneracies. For MAS NMR, the typical assignment protocol relies on a set of complementary 3D ^{13}C detected spectra that include NCOCX, NCaCX, and CONCa (or CaNCO). These experiments provide intra-residue correlations (NCaCX) and inter-residue correlations (NCOCX and CONCa) that, in principle, establish complete backbone and sidechain connectivities. In combination with both selective and extensive labeling, this approach has been applied successfully to a number of systems (Higman et al. 2009; Sperling et al. 2010; Bockmann 2008; Bayro et al. 2010).

One-bond ^{15}N-^{13}C transfers following ^{15}N evolution in NCC experiments are typically achieved with SPECIFIC-CP (Baldus et al. 1998) rather than other N-C recoupling methods such as TEDOR (Hing et al. 1992) or broadband DCP (Schaefer et al. 1979). This is motivated by the fact that SPECIFIC-CP transfers should, in principle, yield the highest transfer efficiencies (theoretically up to 73%). While other heteronuclear recoupling methods have been proposed to compensate for rf imperfections (Kehlet et al. 2007; Hansen et al. 2007) and may arguably perform better than SPECIFIC-CP, SPECIFIC-CP remains the most widely used method. As such, it provides a good benchmark for assessing alternative approaches. Other heteronuclear (primarily ^{13}C-^{15}N) recoupling methods include REDOR (Gullion and Schaefer 1989), FDR (Bennett et al. 1994), SFAM (Fu et al. 1997), RFDRCP (Sun et al. 1995), CN_n^ν and RN_n^ν (Brinkmann and Levitt 2001; Zhao et al. 2001) and PAIN-CP (Lewandowski et al. 2007). The robustness of these sequences can be distinguished by a number of criteria, including chemical shift offset dependence, scaling of the recoupling effect, power stability, and sensitivity to experimental imperfections. It is important to consider such practical differences when selecting mixing schemes for correlation spectroscopy in proteins, particularly when two or more methods are integrated into a single experiment.

An additional consideration arises from molecular motion. While nearly-ideal SPECIFIC-CP transfer efficiencies are reported for rigid crystalline or microcrystalline systems, such as the N-f-MLF-OH peptide (Rienstra et al. 2000) and the GB1 protein (Franks et al. 2005), the situation is very different for non-crystalline systems, including some membrane proteins and amyloid fibrils where the SPECIFIC-CP transfer is adversely affected by molecular motions on the intermediate timescale (Sperling et al. 2010).

ZF-TEDOR and BASE-TEDOR (Jaroniec et al. 2002b) are popular methods for measuring precise long-range intra-molecular (Jaroniec et al. 2002a) and intermolecular (Nieuwkoop and Rienstra 2010) distance constraints. Rienstra and coworkers have also reported success in using short and medium-range TEDOR, combined with 2-^{13}C and 1,3-^{13}C glycerol labeling, to obtain proline and glycine assignments and connectivities in 2D experiments (Sperling et al. 2010). Furthermore, Jaroniec and coworkers showed that a semi-constant-time (SCT)-TEDOR scheme boosts the sensitivity for weak ^{15}N-^{13}C(methyl) signals, permitting selective measurement of distances longer than 3.5 Å in uniformly ^{13}C-^{15}N labeled proteins (Helmus et al. 2008). However, TEDOR has not been widely applied for one-bond transfers in 3D NCC experiments. Although a 2D version of the NCC transfer experiment has been used for assignment of RNAs (Riedel et al. 2005), and the 3D version has recently been implemented for a membrane protein (Andreas et al. 2012), neither of these studies addressed the merits of the TEDOR transfer step relative to other N-C transfer mechanisms.

Here we present detailed comparisons of SPECIFIC-CP and ZF-TEDOR transfer efficiency in uniformly ^{15}N,^{13}C labeled GB1 and GvpA. These data motivate a 3D TEDOR-DARR pulse sequence that allows us to generate simultaneous NCaCX and NCOCX correlations in

a single 3D experiment. The increased sweep width for the second indirect dimension can be easily compensated for by non-uniform sampling (Eddy et al. 2012b; Matsuki et al. 2010; Matsuki et al. 2009) or by simply folding the spectra (Andreas et al. 2012).

Materials and Methods

Sample preparation

Uniformly ^{13}C,^{15}N GB1 was prepared according to previously published protocols (Franks et al. 2005; Schmidt et al. 2007). Uniformly ^{13}C,^{15}N GvpA was prepared according to previously published procedures (Bayro et al. 2012; Sivertsen et al. 2009; Sivertsen et al. 2010). The samples were centrifuged into Varian 3.2 zirconia mm rotors and the drive tips were sealed with epoxy to maintain sample hydration.

1D MAS NMR experiments

The 1D ^{15}N-^{13}C spectra were obtained at a spinning frequency of 13.0 kHz, on a custom-built spectrometer (courtesy of Dr. D. Ruben, Francis Bitter Magnet Laboratory/MIT, Cambridge, MA) operating at 750 MHz ^{1}H Larmor frequency and equipped with a triple-resonance ^{1}H/^{13}C/^{15}N 3.2 mm E-free probe (Bruker Biospin, Billerica MA).

The NCO SPECIFIC-CP condition was optimized to match 2.5 times the rotor frequency (ω_r) on ^{15}N (~32.5 kHz) and $3.5 \times \omega_r$ on ^{13}C (45.5 kHz), with 100 kHz ^{1}H CW decoupling during the transfer. The ^{13}C carrier was set to the middle of the CO region (176 ppm), the ^{15}N carrier to 115 ppm, and the ^{1}H carrier to 4 ppm.

The NCa SPECIFIC-CP condition was optimized to match $1.5 \times \omega_r$ on ^{15}N and $2.5 \times \omega_r$ on ^{13}C, with 100 kHz ^{1}H CW decoupling during the transfer. The ^{13}C carrier was set to 57 ppm, the ^{15}N carrier to 115 ppm, and the ^{1}H carrier to 4 ppm. The optimal NCa contact time was found to be 6 ms for both GB1 and GvpA.

Broadband DCP was optimized for overall (both NCa and NCO) transfer efficiencies. This caused suboptimal NCO and NCa transfers individually, but gave the overall highest simultaneous signal. To achieve this, the ^{13}C carrier was set to 110 ppm, with radio frequency matching conditions of $2.5 \times \omega_r$ on ^{15}N (~32.5 kHz) and $3.5 \times \omega_r$ on ^{13}C (45.5 kHz), and 100 kHz ^{1}H CW decoupling during the transfer. The optimal DCP contact time was found to be 7 ms for both GB1 and GvpA.

The ZF-TEDOR experiments were performed using 50 kHz for both ^{13}C and ^{15}N. The mixing period was optimized to 1.28 ms for one bond ^{15}N-^{13}C transfer. (Jaroniec et al. 2002b).

For all 1D comparisons, 83 kHz TPPM ^{1}H decoupling was used during acquisition (total phase difference,18°; TPPM pulse length 5.8 μs). Chemical shifts were referenced using the DSS scale (Morcombe and Zilm 2003), with adamantane (40.48 ppm for ^{13}C) as a secondary standard. Relative NCO transfer efficiencies were determined by integrating the region from 170 ppm to 182 ppm (omitting the carboxyl peaks) for GB1 and GV, while relative NCa transfer efficiencies were determined by integrating the region from 50 ppm to 63 ppm for GV and 47 ppm to 63 ppm for GB1, assuring that only polarization from Ca carbons was used to evaluate transfer efficiencies.

3D MAS NMR experiments

The TEDOR-DARR pulse sequence for these experiments is shown in Figure 1. In these experiments, the dwell time in the ω_1 dimension was synchronized to twice the rotor period (corresponding to bandwidth of $\omega_R/2$), in order to fold the nitrogen spinning sidebands onto

the centerband and to retain the heteronuclear dipolar recoupling during each TEDOR period. As a consequence, the resonances of the amino terminus of the backbone and the lysine sidechains are folded. The chemical shifts were referenced using the DSS scale (Morcombe and Zilm 2003), with adamantane (40.48 ppm for ^{13}C) as a secondary standard. All the data were processed with the nmrPipe (Delaglio et al. 1995), and subsequently analyzed using Sparky (Goddard and Kneller).

The 3D experiments on GB1 were performed using a custom-built spectrometer (courtesy of Dr. D. Ruben, Francis Bitter Magnet Laboratory/MIT, Cambridge, MA) operating at 700 MHz ^{1}H Larmor frequency and equipped with a triple-resonance $^{1}H/^{13}C/^{15}N$ probe with a 3.2 mm MAS stator ($^{1}H/^{13}C/^{15}N$ Varian-Chemagnetics Palo Alto, CA). The spinning frequency of 13.3 kHz, regulated to ± 5 Hz using a Bruker (Bruker Biospin, Billerica, MA) spinning frequency controller, was set to avoid overlap of rotational resonance of the carbonyl sidebands with the aromatic and aliphatic signals in the acquisition dimension (ω_3). The ^{13}C and ^{15}N $\pi/2$ pulses were 5 µs. TPPM decoupling was 71 kHz (total phase difference,18°; TPPM pulse length 6.8 µs) during gaps between REDOR pulses and 71 kHz (total phase difference 22°; TPPM pulse length 6.8 µs) during evolution and acquisition periods. Mixing periods were 1.2 ms for ZF-TEDOR, optimized for one-bond transfers, and 40 ms for DARR. The 3D data set was acquired using $60 \times 210 \times 1024$ points and dwell times of 150.4, 30 and 16 µs for ω_1, ω_2 and ω_3 respectively. Each FID averaged four scans using a recycle delay of 2.3 s for a total experimental time of 5.5 days.

The 3D experiments on gas vesicles were performed using a Bruker spectrometer (Bruker Biospin, Billerica, MA) operating at 900 MHz ^{1}H Larmor frequency and equipped with a triple-resonance 3.2 mm $^{1}H/^{13}C/^{15}N$ e-free MAS probe (Bruker Biospin, Billerica, MA). The spinning frequency of 16.6 kHz, regulated to ± 2 Hz, was set to avoid overlap of the carbonyl sidebands with the aromatic and aliphatic signals in the acquisition dimension (ω_3). The ^{15}N and ^{13}C $\pi/2$ pulses were 7.1 µs and 3.5 µs, respectively. TPPM decoupling was 83 kHz (total phase difference 18°; TPPM pulse length 5.7 µs) during gaps between REDOR pulses, evolution and acquisition periods. Mixing periods were 1.4 ms for ZF-TEDOR and 40 ms for DARR. The 3D data set was acquired using $56 \times 210 \times 1536$ points and dwell times of 120, 30 and 6 µs for ω_1, ω_2 and ω_3,, respectively. Each FID averaged four scans using a recycle delay of 2.3 s for a total experimental time of 5.2 days.

Results and Discussion

Figure 2 compares polarization transfer by SPECIFIC-CP, broadband DCP and ZF-TEDOR $^{15}N-^{13}C$ transfers for GB1 (top) and GvpA (bottom). As expected, we found that higher $^{15}N-^{13}C$ transfer efficiencies for GB1 were achieved with SPECIFIC-CP. Consistent with previously reported results (Franks et al. 2005), signal intensities for NCO and NCa transfers in GB1 were approximately 55% and 42%, respectively, of those obtained by $^{1}H-^{13}C$ cross-polarization, These efficiencies were approximately 1.6 and 1.45 times greater, respectively, than for one-bond optimized ZF-TEDOR. The situation was significantly different in the case of gas vesicles. The SPECIFIC-CP NCO transfer is only 1.17 times more efficient than one-bond ZF-TEDOR and the NCa transfers are practically identical. Table 1 summarizes these 1D comparisons and corresponding results for DCP. The loss of peak intensity induced by mobility in presence of decoupling is a well known effect that has been observed in $-NH_3^+$ group of alanine (Long et al. 1994), in methyl groups coordinated to tungsten (Maus et al. 1996), and in N-f-MLF-OH (Bajaj et al. 2009). Studies are under way to fully understand this effect.

Figure 3 shows that SPECIFIC-CP is more sensitive than TEDOR to varying levels of ^{1}H decoupling during transfer in GvpA. It follows that power fluctuations during decoupling,

e.g., due to probe detuning, would result in sensitivity loss. This can be a limiting factor at high field and with e-free probes.

In light of the above results, and the ability of TEDOR to implement broadband heteronuclear transfers, 3D NCC experiments were performed using TEDOR, with a mixing time of 1.2 ms chosen to restrict polarization transfer to the carbons directly bonded to nitrogen atoms. For the homonuclear transfer DARR was used with a mixing time of 40 ms chosen to allow polarization to be transferred far enough to detect cross-peaks throughout the sidechains.

Figure 4 shows slices of the GB1 spectrum in the ω_1 ^{15}N plane at 127.7, 116.3 and 118.3 ppm corresponding to the L12, V21 and V54 amides. For both the intra-residue correlations (top) and the inter-residue correlations (bottom), the second mixing spreads the polarization along the full length of the side chain thus allowing optimal resolution of all the ^{13}C signals in a single experiment. The resonances are consistent, within ± 0.2 ppm, with previously published assignments (Franks et al. 2005).

Mobile sequences in proteins usually present weak crosspeaks in SPECIFIC-CP experiments, due to unfavorable intermediate timescale dynamics induced by interference with proton decoupling fields. We therefore examined the performance of the TEDOR-DARR sequence on GvpA, a functional amyloid (Bayro et al. 2012) in which mobility may limit the signal intensity. Figure 5 shows examples of intra-residue and inter-residue correlations for GvpA in the ω_1 ^{15}N planes at 116.6 ppm and 124.2 ppm, corresponding respectively to the S49 and A57 amides. As expected, the resonances are broader than for the microcrystalline GB1, but the side chain correlations are clearly resolved.

A further advantage of the TEDOR-CC experiment is the inclusion of ^{15}N-^{13}C correlations within the sidechains of residues such as tryptophan, arginine and lysine. As shown in Figure 6 for W28, R44 and K55 in GvpA, consistent intra-residue cross-peaks are seen in slices corresponding to the backbone and sidechain nitrogens. TEDOR mixing would also include prolines. However, this capability is not illustrated here because proline is not present in GB1 and the single proline residue in GvpA is in the highly mobile C-terminal sequence.

Conclusions

In conclusion, we have shown that a 3D TEDOR-DARR MAS experiment generates a full set of intra- and inter-residue correlations allowing assignments to be completed in a single experiment. In future work at higher spinning frequencies, a useful variation might be a TEDOR-PAR sequence.

Acknowledgments

References

Ader C, Pongs O, Becker S, Baldus M. Protein dynamics detected in a membrane-embedded potassium channel using two-dimensional solid-state NMR spectroscopy. Biochim Biophys Acta-Biomembranes. 2010; 1798(2):286–290.10.1016/j.bbamem.2009.06.023

Andreas LB, Eddy MT, Chou JJ, Griffin RG. Magic-angle-spinning NMR of the drug resistant S31N M2 proton transporter from influenza A. J Am Chem Soc. 2012; 134(17):7215–7218.10.1021/ja3003606 [PubMed: 22480220]

Andreas LB, Eddy MT, Pielak RM, Chou J, Griffin RG. Magic angle spinning NMR investigation of influenza A M2(18-60): support for an allosteric mechanism of inhibition. J Am Chem Soc. 2010; 132(32):10958–10960.10.1021/ja101537p [PubMed: 20698642]

Bajaj VS, van der Wel PCA, Griffin RG. Observation of a low-temperature, dynamically driven structural transition in a polypeptide by solid-state NMR spectroscopy. J Am Chem Soc. 2009; 131(1):118–128.10.1021/ja8045926 [PubMed: 19067520]

Baldus M, Petkova AT, Herzfeld J, Griffin RG. Cross polarization in the tilted frame: assignment and spectral simplification in heteronuclear spin systems. Mol Phys. 1998; 95(6):1197–1207.10.1080/002689798166215

Bateman DA, Tycko R, Wickner RB. Experimentally derived structural constraints for amyloid fibrils of wild-type transthyretin. Biophys J. 2011; 101(10):2485–2492.10.1016/j.bpj.2011.10.009 [PubMed: 22098747]

Bayro MJ, Daviso E, Belenky M, Griffin RG, Herzfeld J. An amyloid organelle, solid-state NMR evidence for cross-beta assembly of gas vesicles. J Biol Chem. 2012; 287(5):3479–3484.10.1074/jbc.M111.313049 [PubMed: 22147705]

Bayro MJ, Debelouchina GT, Eddy MT, Birkett NR, MacPhee CE, Rosay M, Maas WE, Dobson CM, Griffin RG. Intermolecular structure determination of amyloid fibrils with magic-angle spinning and dynamic nuclear polarization NMR. J Am Chem Soc. 2011; 133(35):13967–13974.10.1021/ja203756x [PubMed: 21774549]

Bayro MJ, Maly T, Birkett NR, MacPhee CE, Dobson CM, Griffin RG. High-resolution MAS NMR analysis of PI3-SH3 amyloid fibrils: backbone conformation and implications for protofilament assembly and structure. Biochemistry. 2010; 49(35):7474–7484.10.1021/bi100864t [PubMed: 20707313]

Bennett AE, Becerra LR, Griffin RG. Frequency-selective heteronuclear recoupling in rotating solids. J Chem Phys. 1994; 100(2):812–814.10.1063/1.466563

Bernstein FC, Koetzle TF, Williams GJB, Meyer EF, Brice MD, Rodgers JR, Kennard O, Shimanouchi T, Tasumi M. Protein data bank - computer-based archival file for macromolecular structures. J Mol Biol. 1977; 112(3):535–542.10.1016/s0022-2836(77)80200-3 [PubMed: 875032]

Bhate MP, Wylie BJ, Tian L, McDermott AE. Conformational dynamics in the selectivity filter of KcsA in response to potassium ion concentration. J Mol Biol. 2010; 401(2):155–166.10.1016/j.jmb.2010.06.031 [PubMed: 20600123]

Bockmann A. 3D protein structures by solid-state NMR spectroscopy: ready for high resolution. Angew Chem Int Ed. 2008; 47(33):6110–6113.10.1002/anie.200801352

Brinkmann A, Levitt MH. Symmetry principles in the nuclear magnetic resonance of spinning solids: heteronuclear recoupling by generalized Hartmann-Hahn sequences. J Chem Phys. 2001; 115(1):357–384.10.1063/1.1377031

Comellas G, Lemkau LR, Zhou DH, George JM, Rienstra CM. Structural intermediates during alpha-synuclein fibrillogenesis on phospholipid vesicles. J Am Chem Soc. 2012; 134(11):5090–5099.10.1021/ja209019s [PubMed: 22352310]

Debelouchina GT, Platt GW, Bayro MJ, Radford SE, Griffin RG. Intermolecular alignment in beta(2)-microglobulin amyloid fibrils. J Am Chem Soc. 2010a; 132(48):17077–17079.10.1021/ja1079871 [PubMed: 21077676]

Debelouchina GT, Platt GW, Bayro MJ, Radford SE, Griffin RG. Magic angle spinning NMR analysis of beta(2)-microglobulin amyloid fibrils in two distinct morphologies. J Am Chem Soc. 2010b; 132(30):10414–10423.10.1021/ja102775u [PubMed: 20662519]

Delaglio F, Grzesiek S, Vuister GW, Zhu G, Pfeifer J, Bax A. Nmrpipe - a multidimensional spectral processing system based on unix pipes. J Biomol NMR. 1995; 6(3):277–293.10.1007/bf00197809 [PubMed: 8520220]

Eddy MT, Ong T-C, Clark L, Teijido O, van der Wel PCA, Garces R, Wagner G, Rostovtseva TK, Griffin RG. Lipid dynamics and protein-lipid interactions in 2D crystals formed with the beta-barrel integral membrane protein VDAC1. J Am Chem Soc. 2012a; 134(14):6375–6387.10.1021/ja300347v [PubMed: 22435461]

Eddy MT, Ruben D, Griffin RG, Herzfeld J. Deterministic schedules for robust and reproducible non-uniform sampling in multidimensional NMR. J Magn Reson. 2012b; 214:296–301.10.1016/j.jmr.2011.12.002 [PubMed: 22200565]

Franks WT, Zhou DH, Wylie BJ, Money BG, Graesser DT, Frericks HL, Sahota G, Rienstra CM. Magic-angle spinning solid-state NMR spectroscopy of the beta 1 immunoglobulin binding domain of protein G (GB1): N-15 and C-13 chemical shift assignments and conformational analysis. J Am Chem Soc. 2005; 127(35):12291–12305.10.1021/ja044497e [PubMed: 16131207]

Fu RQ, Smith SA, Bodenhausen G. Recoupling of heteronuclear dipolar interactions in solid state magic-angle spinning NMR by simultaneous frequency and amplitude modulation. Chem Phys Lett. 1997; 272(5–6):361–369.10.1016/s0009-2614(97)00537-x

Goddard, TD.; Kneller, DG. University of California; San Francisco, CA:

Gullion T, Schaefer J. Rotational-echo double-resonance nmr. J Magn Reson. 1989; 81(1):196–200.10.1016/0022-2364(89)90280-1

Hansen JO, Kehlet C, Bjerring M, Vosegaard T, Glaser SJ, Khaneja N, Nielsen NC. Optimal control based design of composite dipolar recoupling experiments by analogy to single-spin inversion pulses. Chem Phys Lett. 2007; 447(1–3):154–161.10.1016/j.cplett.2007.08.072

Helmus JJ, Nadaud PS, Hofer N, Jaroniec CP. Determination of methyl C-13-N-15 dipolar couplings in peptides and proteins by three-dimensional and four-dimensional magic-angle spinning solid-state NMR spectroscopy. J Chem Phys. 2008; 128(5):052314/1–16.10.1063/1.2817638 [PubMed: 18266431]

Higman VA, Flinders J, Hiller M, Jehle S, Markovic S, Fiedler S, van Rossum B-J, Oschkinat H. Assigning large proteins in the solid state: a MAS NMR resonance assignment strategy using selectively and extensively C-13-labelled proteins. J Biomol NMR. 2009; 44(4):245–260.10.1007/s10858-009-9338-7 [PubMed: 19609683]

Higman VA, Varga K, Aslimovska L, Judge PJ, Sperling LJ, Rienstra CM, Watts A. The Conformation of bacteriorhodopsin loops in purple membranes resolved by solid-state MAS NMR spectroscopy. Angew Chem Int Ed. 2011; 50(36):8432–8435.10.1002/anie.201100730

Hing AW, Vega S, Schaefer J. Transferred-echo double-resonance NMR. J Magn Reson. 1992; 96(1):205–209.10.1016/0022-2364(92)90305-q

Hu K-N, McGlinchey RP, Wickner RB, Tycko R. Segmental polymorphism in a functional amyloid. Biophys J. 2011; 101(9):2242–2250.10.1016/j.bpj.2011.09.051 [PubMed: 22067164]

Jaroniec CP, MacPhee CE, Astrof NS, Dobson CM, Griffin RG. Molecular conformation of a peptide fragment of transthyretin in an amyloid fibril. P Natl Acad Sci USA. 2002a; 99(26):16748–16753.10.1073/pnas.252625999

Jaroniec CP, Filip C, Griffin RG. 3D TEDOR NMR experiments for the simultaneous measurement of multiple carbon-nitrogen distances in uniformly C-13, N-15-labeled solids. J Am Chem Soc. 2002b; 124(36):10728–10742.10.1021/ja026385y [PubMed: 12207528]

Kehlet C, Bjerring M, Sivertsen AC, Kristensen T, Enghild JJ, Glaser SJ, Khaneja N, Nielsen NC. Optimal control based NCO and NCA experiments for spectral assignment in biological solid-state NMR spectroscopy. J Magn Reson. 2007; 188(2):216–230.10.1016/j.jmr.2007.06.011 [PubMed: 17681479]

Kryndushkin DS, Wickner RB, Tycko R. The Core of Ure2p Prion fibrils is formed by the N-terminal segment in a parallel cross-beta structure: evidence from solid-state NMR. J Mol Biol. 2011; 409(2):263–277.10.1016/j.jmb.2011.03.067 [PubMed: 21497604]

Lemkau LR, Comellas G, Kloepper KD, Woods WS, George JM, Rienstra CM. Mutant protein A30P alpha-synuclein adopts wild-type fibril structure, despite slower fibrillation kinetics. J Biol Chem. 2012; 287(14):11526–11532.10.1074/jbc.M111.306902 [PubMed: 22334684]

Lewandowski JR, De Paepe G, Griffin RG. Proton assisted insensitive nuclei cross polarization. J Am Chem Soc. 2007; 129(4):728–729.10.1021/ja0650394 [PubMed: 17243786]

Li J, Hoop CL, Kodali R, Sivanandam VN, van der Wel PCA. Amyloid-like fibrils from a domain-swapping protein feature a parallel, in-register conformation without native-like interactions. J Biol Chem. 2011; 286(33):28988–28995.10.1074/jbc.M111.261750 [PubMed: 21715337]

Li Y, Berthold DA, Gennis RB, Rienstra CM. Chemical shift assignment of the transmembrane helices of DsbB, a 20-kDa integral membrane enzyme, by 3D magic-angle spinning NMR spectroscopy. Protein Sci. 2008; 17(2):199–204.10.1110/ps.073225008 [PubMed: 18227427]

Long JR, Sun BQ, Bowen A, Griffin RG. Molecular dynamics and magic-angle-spinning NMR. J Am Chem Soc. 1994; 116(26):11950–11956.10.1021/ja00105a039

Lv G, Kumar A, Giller K, Orcellet ML, Riedel D, Fernandez CO, Becker S, Lange A. Structural comparison of mouse and human alpha-synuclein amyloid fibrils by solid-state NMR. J Mol Biol. 2012; 420(1–2):99–111.10.1016/j.jmb.2012.04.009 [PubMed: 22516611]

Matsuki Y, Eddy MT, Griffin RG, Herzfeld J. Rapid three-dimensional MAS NMR spectroscopy at critical sensitivity. Angew Chem Int Ed. 2010; 49(48):9215–9218.10.1002/anie.201003329

Matsuki Y, Eddy MT, Herzfeld J. Spectroscopy by integration of frequency and time domain information for fast acquisition of high-resolution dark spectra. J Am Chem Soc. 2009; 131(13): 4648–4656.10.1021/ja807893k [PubMed: 19284727]

Maus DC, Copie V, Sun BQ, Griffiths JM, Griffin RG, Luo SF, Schrock RR, Liu AH, Seidel SW, Davis WM, Grohmann A. A solid-state NMR study of tungsten methyl group dynamics in W(eta(5)-C(5)Me(5))Me(4) PF6. J Am Chem Soc. 1996; 118(24):5665–5671.10.1021/ja960248h

Morcombe CR, Zilm KW. Chemical shift referencing in MAS solid state NMR. J Magn Reson. 2003; 162(2):479–486.10.1016/s1090-7807(03)00082-x [PubMed: 12810033]

Nieuwkoop AJ, Rienstra CM. Supramolecular protein structure determination by site-specific long-range intermolecular solid state NMR Spectroscopy. J Am Chem Soc. 2010; 132(22):7570–7571.10.1021/ja100992y [PubMed: 20465251]

Paravastu AK, Leapman RD, Yau W-M, Tycko R. Molecular structural basis for polymorphism in Alzheimer's beta-amyloid fibrils. P Natl Acad Sci USA. 2008; 105(47):18349–18354.10.1073/pnas.0806270105

Paravastu AK, Qahwash I, Leapman RD, Meredith SC, Tycko R. Seeded growth of beta-amyloid fibrils from Alzheimer's brain-derived fibrils produces a distinct fibril structure. P Natl Acad Sci USA. 2009; 106(18):7443–7448.10.1073/pnas.0812033106

Qiang W, Yau W-M, Luo Y, Mattson MP, Tycko R. Antiparallel beta-sheet architecture in Iowa-mutant beta-amyloid fibrils. P Natl Acad Sci USA. 2012; 109(12):4443–4448.10.1073/pnas.1111305109

Renault M, Bos MP, Tommassen J, Baldus M. Solid-State NMR on a large multidomain integral membrane protein: the outer membrane protein assembly factor BamA. J Am Chem Soc. 2011; 133(12):4175–4177.10.1021/ja109469c [PubMed: 21361323]

Riedel K, Leppert J, Ohlenschlager O, Gorlach M, Ramachandran R. TEDOR with adiabatic inversion pulses: resonance assignments of C-13/N-15 labelled RNAs. J Biomol NMR. 2005; 31(1):49–57.10.1007/s10858-004-6066-x [PubMed: 15692738]

Rienstra CM, Hohwy M, Hong M, Griffin RG. 2D and 3D N-15-C-13-C-13 NMR chemical shift correlation spectroscopy of solids: assignment of MAS spectra of peptides. J Am Chem Soc. 2000; 122(44):10979–10990.10.1021/ja001092v

Schaefer J, McKay RA, Stejskal EO. Double-cross-polarization nmr of solids. J Magn Reson. 1979; 34(2):443–447.10.1016/0022-2364(79)90022-2

Schmidt HLF, Sperling LJ, Gao YG, Wylie BJ, Boettcher JM, Wilson SR, Rienstra CA. Crystal polymorphism of protein GB1 examined by solid-state NMR spectroscopy and X-ray diffraction. J Phys Chem B. 2007; 111(51):14362–14369.10.1021/jp075531p [PubMed: 18052145]

Sivanandam VN, Jayaraman M, Hoop CL, Kodali R, Wetzel R, van der Wel PCA. The aggregation-enhancing Huntingtin N-terminus is helical in amyloid fibrils. J Am Chem Soc. 2011; 133(12): 4558–4566.10.1021/ja110715f [PubMed: 21381744]

Sivertsen AC, Bayro MJ, Belenky M, Griffin RG, Herzfeld J. Solid-State NMR evidence for inequivalent GvpA subunits in gas vesicles. J Mol Biol. 2009; 387(4):1032–1039.10.1016/j.jmb. 2009.02.015 [PubMed: 19232353]

Sivertsen AC, Bayro MJ, Belenky M, Griffin RG, Herzfeld J. Solid-state NMR characterization of gas vesicle structure. Biophys J. 2010; 99(6):1932–1939.10.1016/j.bpj.2010.06.041 [PubMed: 20858439]

Sperling LJ, Berthold DA, Sasser TL, Jeisy-Scott V, Rienstra CM. Assignment strategies for large proteins by magic-angle spinning NMR: The 21-kDa disulfide-bond-forming enzyme DsbA. J Mol Biol. 2010; 399(2):268–282.10.1016/j.jmb.2010.04.012 [PubMed: 20394752]

Sun BQ, Costa PR, Kocisko D, Lansbury PT, Griffin RG. Internuclear distance measurements in solid-state nuclear-magnetic-resonance - dipolar recoupling via rotor synchronized spin locking. J Chem Phys. 1995; 102(2):702–707.10.1063/1.469182

Van Melckebeke H, Wasmer C, Lange A, Ab E, Loquet A, Bockmann A, Meier BH. Atomic-resolution three-dimensional structure of HET-s(218-289) amyloid fibrils by solid-state NMR spectroscopy. J Am Chem Soc. 2010; 132(39):13765–13775.10.1021/ja104213J [PubMed: 20828131]

Varga K, Tian L, McDermott AE. Solid-state NMR study and assignments of the KcsA potassium ion channel of S. lividans. Biochim Biophys Acta-Proteins and Proteomics. 2007; 1774(12):1604–1613.10.1016/j.bbapap.2007.08.029

Warschawski, D. Proteins of known structure determined by solid-State NMR. 2011. http://www.drorlist.com/nmr/SPNMR.html

Wasmer C, Lange A, Van Melckebeke H, Siemer AB, Riek R, Meier BH. Amyloid fibrils of the HET-s(218-289) prion form a beta solenoid with a triangular hydrophobic core. Science. 2008; 319(5869):1523–1526.10.1126/science.1151839 [PubMed: 18339938]

Zhao X, Eden M, Levitt MH. Recoupling of heteronuclear dipolar interactions in solid-state NMR using symmetry-based pulse sequences. Chem Phys Lett. 2001; 342(3–4):353–361.10.1016/s0009-2614(01)00593-0
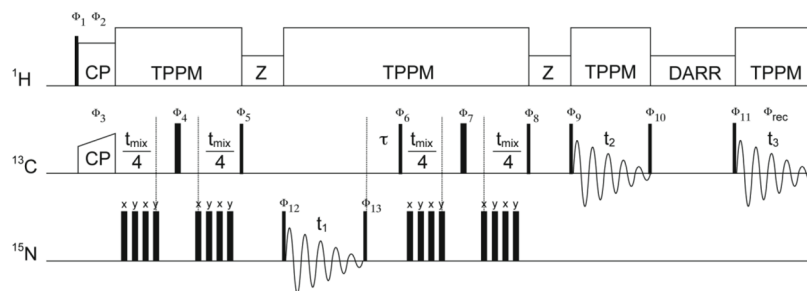
Figure 1.
The 3D NCC *z*-filtered TEDOR-DARR pulse sequence. Narrow and wide filled rectangles represent $\pi/2$ and π pulses, respectively. During the TEDOR mixing, π pulses are applied on the ^{15}N channel and phase cycled according to the *xy*-4 scheme. The short delay, τ, after the f_1 ^{15}N evolution period ensures that the total delay between the REDOR mixing periods is equal to an integer of rotor cycles as required for efficient reconversion of the anti-phase coherences into observable ^{13}C magnetization. In the experiment presented here, the value of τ was set to in order to maintain rotor synchronization since the dwell time for the f_1 ^{15}N dimension has been chosen to be exactly two rotor periods. During the z-filters and the DARR mixing time, a weak proton field, $\omega_{rf} = \omega_r$, was applied to facilitate the rapid dephasing of transverse ^{13}C spin coherences and to promote proton driven spin diffusion of z-magnetization of ^{13}C spin population, respectively. The adopted phase cycles are: $\Phi_1 = 1111$, $\Phi_2 = 2222$, $\Phi_3 = \Phi_6 = 1111$, $\Phi_4 = \Phi_7 = 1111$, $\Phi_5 = 1111$, $\Phi_8 = 2244$, $\Phi_9 = 1111$, $\Phi_{10} = 2244$, $\Phi_{11} = 1111$, $\Phi_{12} = 1111$, $\Phi_{13} = 1313$, and $\Phi_{rec} = 4224$.
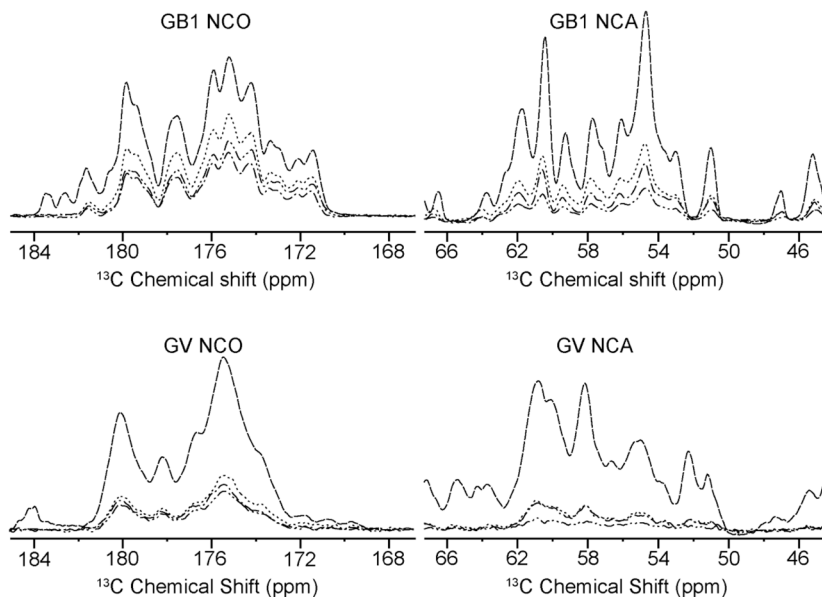
Figure 2.
1D ^{13}C detected comparison of ^{15}N-^{13}C transfer methods for GB1 (top) and Gvpa (bottom) in the CO (left) and Ca regions (right). 1D ^{13}C CP only (dash), SPECIFIC-CP (dot), broadband DCP (dash-dot-dot), and one-bond optimized ZF-TEDOR (dash-dot). 100 kHz ^1H decoupling was used during all the ^{15}N-^{13}C recoupling periods.
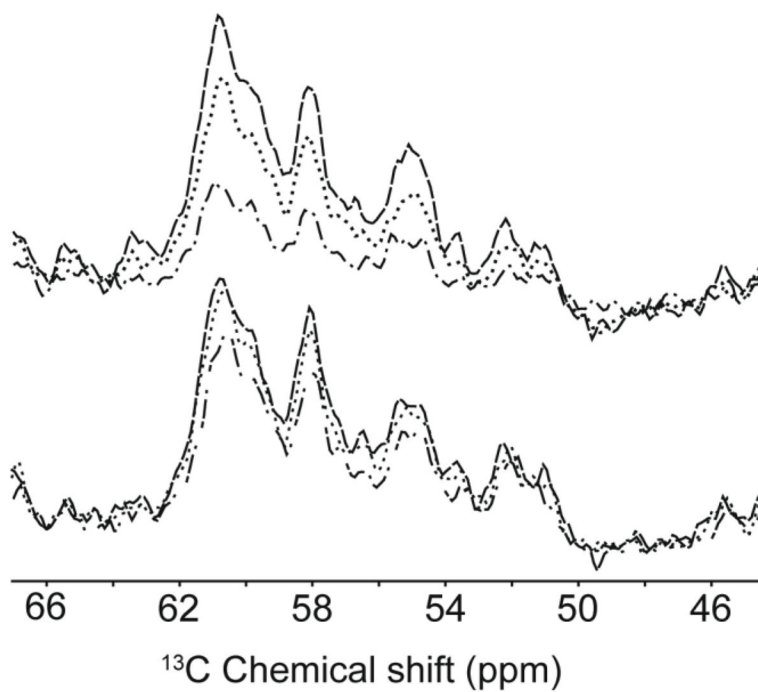
Figure 3.
1D ^{13}C detected comparisons of ^{15}N-^{13}C heteronuclear transfer at varying levels of ^{1}H decoupling in GvpA. Top: SPECIFIC-CP NCa with 100 kHz (dash), 83 kHz (dot), and 71 kHz (dash-dot) ^{1}H decoupling. Bottom: 1.28 ms TEDOR with 100 kHz (dash), 83 kHz (dot), and 71 kHz (dash-dot) ^{1}H decoupling.
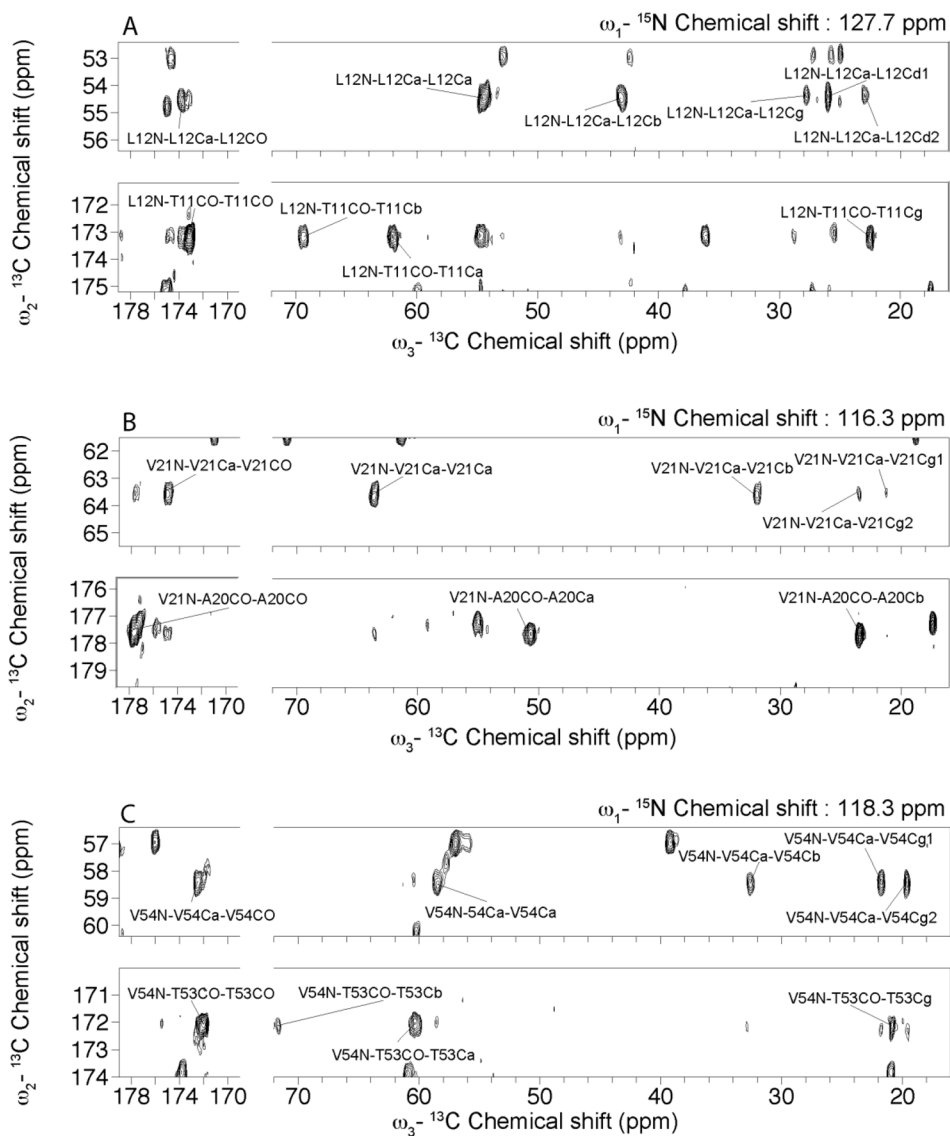
Figure 4.
Slices of the ZF-TEDOR-DARR spectrum of GB1 at the ^{15}N frequencies of the L12 (A), V21 (B) and V54 (C) amides.
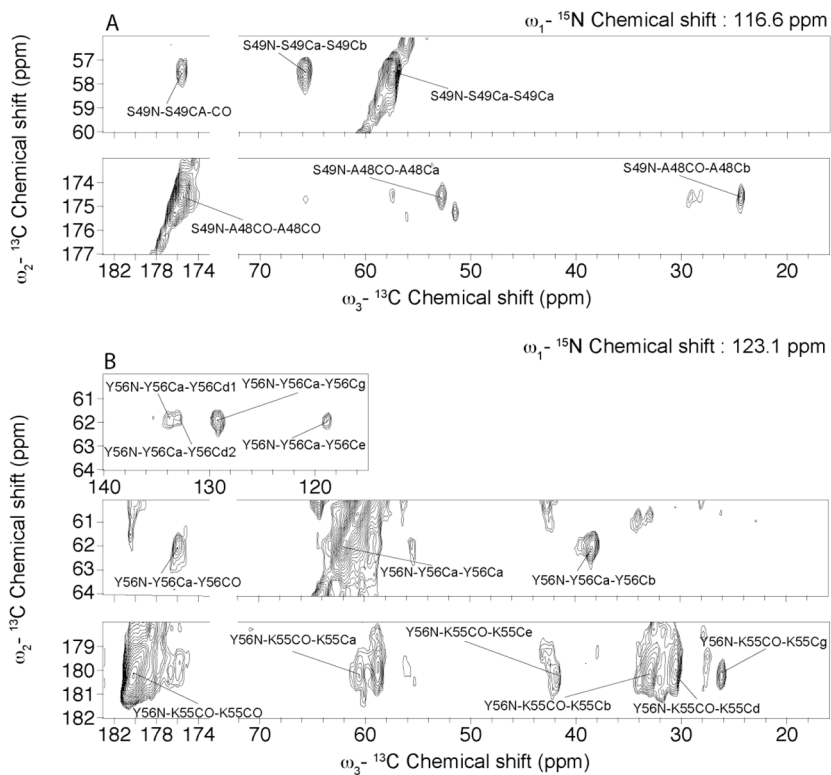
Figure 5.
Slices of the ZF-TEDOR-DARR spectrum of GvpA at the ^{15}N frequencies of the S49 (A) and Y56 (B) amides.
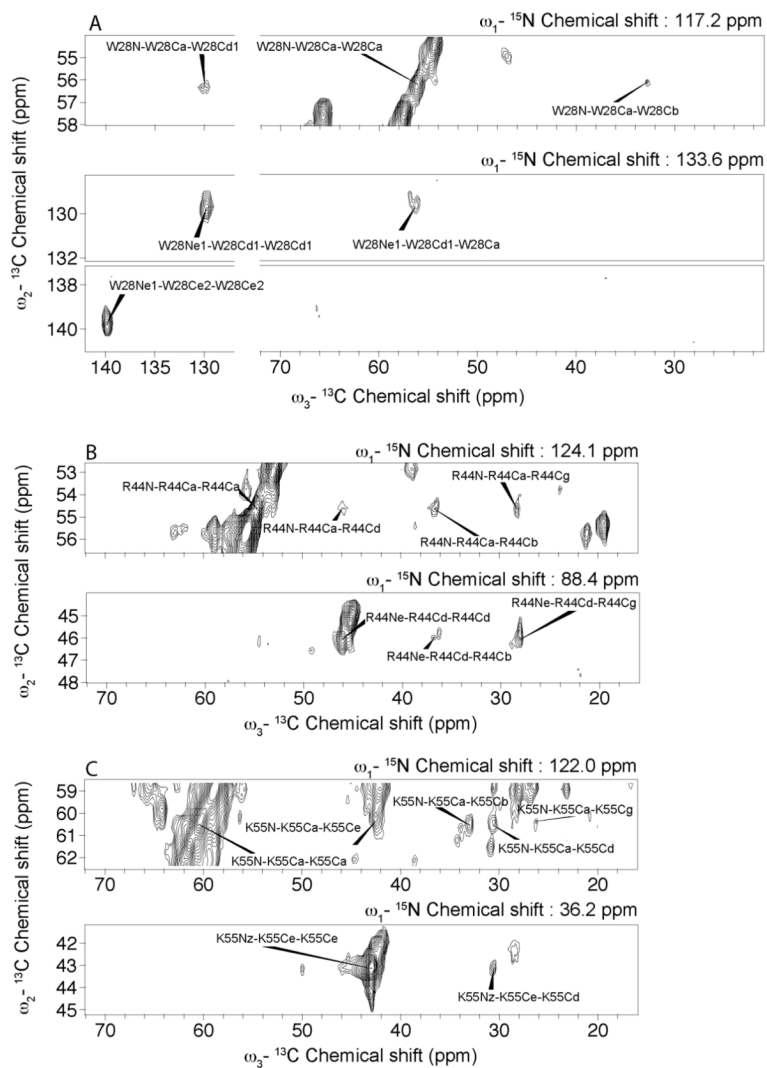
Figure 6.
Sidechain correlations by ^{15}N-^{13}C polarization transfer from both backbone and sidechain nitrogens in W28 (A), R44 (B) and K55 (C) of GvpA.

Table 1

Relative ^{15}N-^{13}C transfer efficiencies for GB1 and GvpA.

Sample	^{13}C CP	SPECIFIC CP NCa	SPECIFIC CP NCO	Broadband DCP NCa	Broadband DCP NCO	ZF-TEDOR NCa	ZF-TEDOR NCO
GB1	1.0	0.42	0.55	0.17	0.41	0.29	0.34
GvpA	1.0	0.19	0.27	0.05	0.20	0.18	0.23